structure is a frequent prediction of coupled spin-charge order theories for the cuprates (*2*, *3*, *6–8*, *32–34*) but has not been previously observed in the quasi-particle spectrum of any HTSC system. Second, some degree of one-dimensionality is evident in these incommensurate LDOS modulations because one Cu-O direction has stronger spectral intensity than the other. Finally, the vortex-induced LDOS is detected by STM at least 50 Å away from the core. This means that, at only 5 T, ~25% of the sample is under the influence of whatever phenomenon generates the checkerboard of LDOS modulations, even though the vortex cores themselves make up only ~2% of its area.

References and Notes

1. I. Affleck, J. B. Marston, *Phys. Rev. B* **37**, 3774 (1988).
2. J. Zaanen, O. Gunnarsson, *Phys. Rev. B* **40**, 7391 (1989).
3. U. Löw *et al*., *Phys. Rev. Lett.* **72**, 1918 (1994).
4. X.-G. Wen, P. A. Lee, *Phys. Rev. Lett.* **76**, 503 (1996).
5. S.-C. Zhang, *Science* **275**, 1089 (1997).
6. O. Zachar *et al*., *Phys. Rev. B* **57**, 1422 (1998).
7. V. J. Emery, S. A. Kivelson, J. M. Tranquada, *Proc. Natl. Acad. Sci. U.S.A.* **96**, 8814 (1999).
8. M. Vojta, S. Sachdev, *Phys. Rev. Lett.* **83**, 3916 (1999).
9. C. M. Varma, *Phys. Rev. B* **61**, R3804 (2000).
10. S. Chakravarty *et al*., *Phys. Rev. B* **63**, 094503 (2001).
11. J. L. Tallon, J. W. Loram, *Physica C* **349**, 53 (2001).
12. Y. Ando *et al*., *Phys. Rev. Lett.* **75**, 4662 (1995).
13. G. S. Boebinger *et al.*, *Phys. Rev. Lett.* **77**, 5417 (1996).
14. G. E. Volovik, *JETP Lett.* **58**, 469 (1993).
15. P. I. Soininen *et al*., *Phys. Rev. B* **50**, 13883 (1994).
16. Y. Wang, A. H. MacDonald, *Phys. Rev. B* **52**, R3876 (1995).
17. M. Ichioka *et al*., *Phys. Rev. B* **53**, 15316 (1996).
18. M. Franz, Z. Tešanović, *Phys. Rev. Lett.* **80**, 4763 (1998).
19. I. Maggio-Aprile *et al*., *Phys. Rev. Lett.* **75**, 2754 (1995).
20. Ch. Renner *et al*., *Phys. Rev. Lett.* **80**, 3606 (1998).
21. S. H. Pan *et al.*, *Phys. Rev. Lett.* **85**, 1536 (2000).
22. D. P. Arovas *et al*., *Phys. Rev. Lett.* **79**, 2871 (1997).
23. E. Demler *et al*., *Phys. Rev. Lett.* **87**, 067202 (2001).
24. J.-i. Kishine *et al*., *Phys. Rev. Lett.* **86**, 5365 (2001).
25. J.-X. Zhu, C. S. Ting, *Phys. Rev. Lett.* **87**, 147002 (2001).
26. Q.-H. Wang *et al*., *Phys. Rev. Lett.* **87**, 167004(2001).
27. B. Lake *et al.*, *Science* **291**, 1759 (2001).
28. B. Khaykovich *et al.*, preprint available at xxx.lanl.gov/abs/cond-mat/0112505.
29. V. F. Mitrović *et al.*, *Nature* **413**, 501 (2001).
30. J.-P. Hu, S.-C. Zhang, *J. Phys. Chem. Solids*, in press.
31. K. Park, S. Sachdev, *Phys. Rev. B* **64**, 184510 (2001).
32. S. R. White, D. J. Scalapino, *Phys. Rev. Lett.* **80**, 1272 (1998).
33. S. A. Kivelson, E. Fradkin, V. J. Emery, *Nature* **393**, 550 (1998).
34. J. Zaanen, *Nature* **404,** 714 (2000).

35. We acknowledge and thank S. Sachdev, S. Kivelson, D.-H. Lee, E. Demler, S.-C. Zhang, J. Sethna, G. Aeppli, J. Orenstein, W. Halperin, and S. H. Pan for helpful conversations and communications. This work was funded by the Office of Naval Research, the Materials Sciences Division of Lawrence Berkeley National Laboratory, the CULAR Program of Los Alamos National Laboratory, as well as a Grant-in-Aids for Scientific Research, a COE Grant from the Ministry of Education, and an International Joint Research Grant from the New Energy and Industrial Technology Organization in Japan. J.E.H. acknowledges support by a Hertz Fellowship, K.M.L. by an IBM Fellowship, and J.C.D. by a Miller Professorship.

9 October 2001; accepted 10 December 2001

Systematic Design of Pore Size and Functionality in Isoreticular MOFs and Their Application in Methane Storage

Mohamed Eddaoudi,[1] Jaheon Kim,[1] Nathaniel Rosi,[1] David Vodak,[1] Joseph Wachter,[1] Michael O'Keeffe,[2] Omar M. Yaghi[1]*

A strategy based on reticulating metal ions and organic carboxylate links into extended networks has been advanced to a point that allowed the design of porous structures in which pore size and functionality could be varied systematically. Metal-organic framework (MOF-5), a prototype of a new class of porous materials and one that is constructed from octahedral Zn-O-C clusters and benzene links, was used to demonstrate that its three-dimensional porous system can be functionalized with the organic groups –Br, $–NH_2$, $–OC_3H_7$, $–OC_5H_{11}$, $–C_2H_4$, and $–C_4H_4$ and that its pore size can be expanded with the long molecular struts biphenyl, tetrahydropyrene, pyrene, and terphenyl. We synthesized an isoreticular series (one that has the same framework topology) of 16 highly crystalline materials whose open space represented up to 91.1% of the crystal volume, as well as homogeneous periodic pores that can be incrementally varied from 3.8 to 28.8 angstroms. One member of this series exhibited a high capacity for methane storage (240 cubic centimeters at standard temperature and pressure per gram at 36 atmospheres and ambient temperature), and others the lowest densities (0.41 to 0.21 gram per cubic centimeter) for a crystalline material at room temperature.

An outstanding challenge in the synthesis of crystalline solid state materials is to alter chemical composition, functionality, and molecular dimensions systematically, that is, without changing the underlying topology (*1*, *2*). The insolubility of extended solids necessitates that their assembly be accomplished in a single step (*3*). Thus, in order to design a target extended structure with the same precision practiced in organic synthesis, (i) the starting building blocks should have the relevant attributes necessary to assemble the skeleton of the desired structure, (ii) the synthesis must be adaptable to the use of derivatives of those building blocks to produce structures with the same skeleton but different functionalities and dimensions, and (iii) the products should be highly crystalline to facilitate their characterization by x-ray diffraction (XRD) techniques.

We and others have pursued the assembly of extended structures of metal-organic frameworks (MOFs) from molecular building blocks (*4–9*). In MOF-5, octahedral Zn-O-C clusters are linked by benzene struts to reticulate a primitive cubic structure (Fig. 1, **1**) (*9*) and produce an exceptionally rigid and highly porous structure. Here we report the systematic design and construction of a series of frameworks that have structures based on the skeleton of MOF-5, wherein the pore functionality and size have been varied without changing the original cubic topology. Several members of this series have pore sizes in the mesoporous range (>20 Å) as well as the lowest crystal density of any material reported to date. One of these compounds, isoreticular MOF–6 (IRMOF-6), has the highest methane storage capacity measured thus far.

The design of an IRMOF (*10*) series based on MOF-5 was initiated by determining the reaction conditions necessary to produce the octahedral cluster with a ditopic linear carboxylate link in situ. In this context, the original low-yielding synthesis of MOF-5 was re-examined and developed into a high-yielding preparation: An *N*,*N*′-diethylformamide (DEF) solution mixture of $Zn(NO_3)_2{\cdot}4H_2O$ and the acid form of 1,4-benzenedicarboxylate (BDC) are heated (85° to 105°C) in a closed vessel to give crystalline MOF-5, $Zn_4O(R_1\text{-BDC})_3$ (where

[1]Materials Design and Discovery Group, Department of Chemistry, University of Michigan, Ann Arbor, MI 48109, USA. [2]Materials Design and Discovery Group, Department of Chemistry, Arizona State University, Tempe, AZ 85287, USA.

*To whom correspondence should be addressed. E-mail: oyaghi@umich.edu

R_1 = H), hereafter termed IRMOF-1, in 90% yield.

The simplicity of the method and the facility with which IRMOF-1 can be obtained indicated that the use of other ditopic carboxylate links (Scheme 1) under closely related, if not identical, conditions would yield the same type of frameworks with diverse pore sizes and functionalities. Indeed, using each of the links R_2-BDC, R_3-BDC, R_4-BDC, R_5-BDC, R_6-BDC, R_7-BDC, 2,6-NDC, BPDC, HPDC, PDC, and TPDC instead of BDC yielded IRMOF-2 through -16, including the noninterpenetrating structures of BPDC, HPDC, PDC, and TPDC. Each member of the IRMOF series has been isolated and was formulated subsequently by chemical microanalysis and single-crystal XRD studies (*11*, *12*).

All IRMOFs have the expected topology of CaB_6 (*13*) adapted by the prototype IRMOF-1 (Fig. 1, **1**) in which an oxide-centered Zn_4O tetrahedron is edge-bridged by six carboxylates to give the octahedron-shaped secondary building unit (SBU) that reticulates into a three-dimensional (3D) cubic porous network. However, the IRMOFs differ in the nature of functional groups decorating the pores and in the metrics of their pore structure. In IRMOF-2 through -7, BDC links with bromo, amino, *n*-propoxy, *n*-pentoxy, cyclobutyl, and fused benzene functional groups reticulate into the desired structure wherein the groups point into the voids (Fig. 1, **2** to **7**). Thus, we can use a wide variety of carboxylate links diverse in their functional groups—rare aspects that heretofore remained largely absent in crystalline solid state and porous materials research. Pore expansion is also within the scope of this chemistry, as illustrated by the structures of IRMOF-8 through -16 (Fig. 1), in which progressively longer links have been successfully used.

Previous geometric analysis of the primitive cubic system showed that expansion of links results in interpenetrating frameworks, sometimes with optimal porosity (*14*). In fact, with the exception of the noninterpenetrating structure involving 2,6-NDC (IRMOF-8) (Fig. 1, **8**), BPDC, HPDC, PDC, and TPDC (IRMOF-9, -11, -13, and -15, respectively) are each reticulated as doubly interpenetrating structures. However, by carrying out the original reactions under more dilute conditions, noninterpenetrating counterparts have been successfully achieved for all links including TPDC (IRMOF-10, -12, -14, and -16) (Fig. 1, **10**, **12**, **14**, and **16**). Thus, our strategies have allowed the synthesis of both interpenetrating and noninterpenetrating forms of the same extended structure.

Comparison of the percent free volume in crystals of IRMOF-1 through -16 (Fig. 2) shows that it varies in small increments (1 to 5%) from 55.8% in IRMOF-5 to 91.1% in IRMOF-16. Remarkably, the lowest percent free volume obtained in this series exceeds that found in some of the most open zeolites, such as faujasite (*15*) in which the free space is 45 to 50% of the crystal volume. In fact,

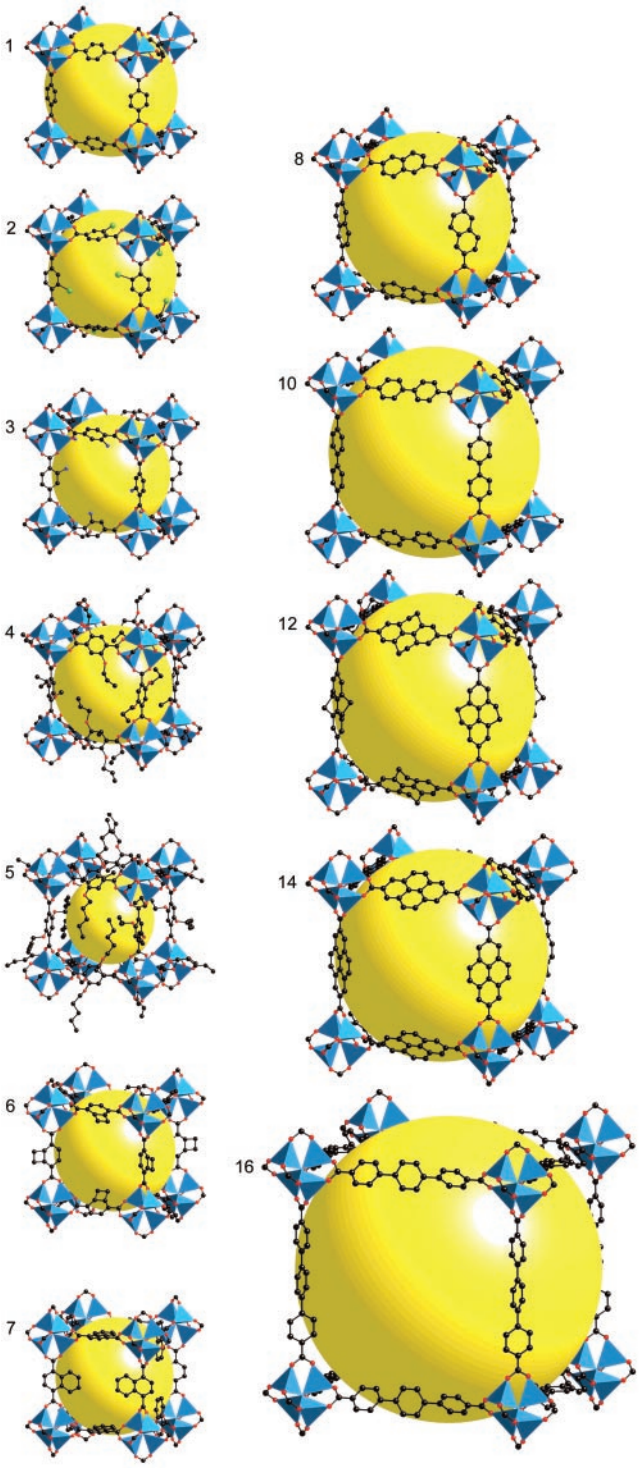

Fig. 1. Single crystal x-ray structures of IRMOF-n (n = 1 through 7, 8, 10, 12, 14, and 16), labeled respectively. The doubly interpenetrated IRMOFs (9, 11, 13, and 15) are not shown [see text and (*23*)]. Color scheme is as follows: Zn (blue polyhedra), O (red spheres), C (black spheres), Br (green spheres in **2**), amino-groups (blue spheres in **3**). The large yellow spheres represent the largest van der Waals spheres that would fit in the cavities without touching the frameworks. All hydrogen atoms have been omitted, and only one orientation of disordered atoms is shown for clarity.

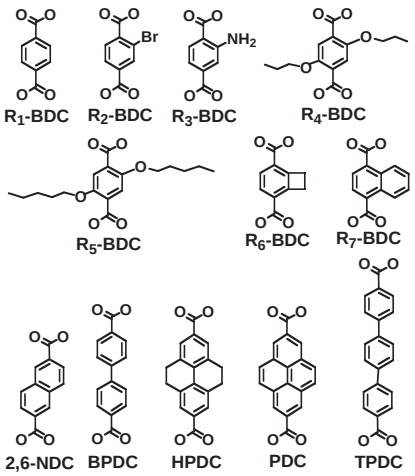

Scheme 1.

the fraction of free space in crystals of the expanded IRMOF series, especially those of IRMOF-8, -10, -12, -14, and -16, has only been achievable in non-crystalline porous systems such as SiO_2 xerogels and aerogels (*16*).

The calculated crystal densities (in the absence of guests) of these materials also vary in small increments (~0.1) in the range 1.00 g/cm^3 for IRMOF-5 to 0.21 g/cm^3 for IRMOF-16 (Fig. 2). Moreover, the densities of IRMOF-8, -10, -12, -14, -15, and -16 are the lowest reported for any crystalline material known to date. In comparison, the density of Li metal is 0.56 g/cm^3.

As expected, the impact of functionalization on pore dimensions is pronounced: relative to IRMOF-1, both the free and fixed diameters of the pores in IRMOF-2 through -7 are modulated downward at ~2 Å intervals in the respective ranges, 11.2 to 3.8 Å and 18.6 to 12.8 Å (Fig. 2). A similar trend is also observed for the interpenetrating structures, where pore sizes that fall below those of the IRMOF-1 are obtained. However, all of the expanded noninterpenetrating structures have free- and fixed-diameter values that are much higher, falling within the respective ranges 12.6 to 19.1 Å and 21.4 to 28.8 Å (Fig. 2). The latter upper limit is in the mesoporous range, indicating the likelihood that such reticular chemistry may be used more routinely toward the design and synthesis of crystalline and fully ordered mesoporous crystals.

Given the exceptional attributes of such materials, including their thermal stability, periodicity (the ability to append functional groups in the pores), and the demonstrated systematic variation in pore size and porosity, it is expected that each member of this series would exhibit an unusually rich inclusion chemistry. Our initial results in methane storage provide a glimpse into the vast potential of IRMOFs.

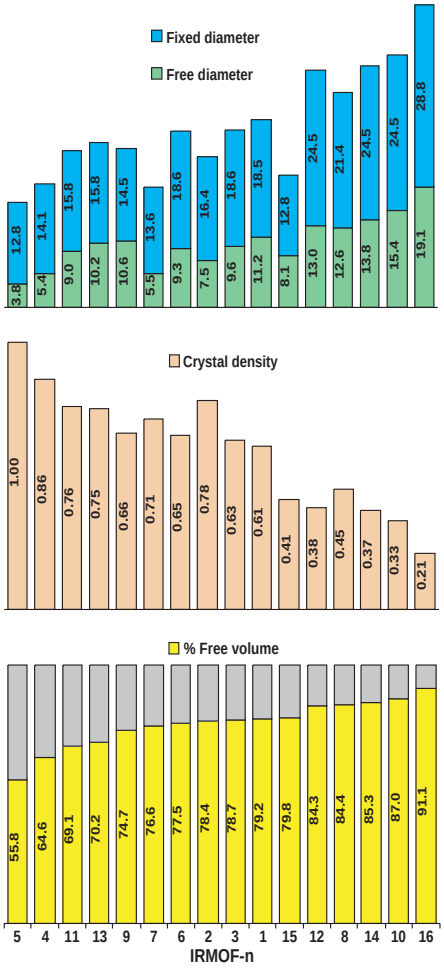

Fig. 2. (Bottom to top) For IRMOF-1 through -16, the calculated (using the program cerius^2, version 4.2) percent free volume (yellow), crystal densities (light brown), and free diameter (green) and fixed diameter (blue), respectively, were obtained by measuring the diameter of a sphere that would pass through the aperture and another that would fit inside the pores without overlapping with framework atoms.

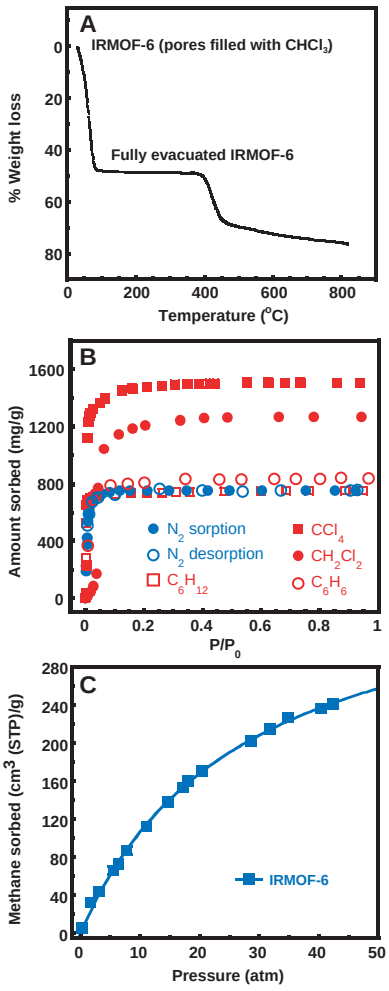

Fig. 3. (**A**) Thermogravimetrogram for IRMOF-6 including its (**B**) gas and organic vapor sorption isotherms and (**C**) its voluminous uptake of methane gas fitted at 298 K with Langmuir equation.

The use of methane as a potential fuel has been a long-standing challenge because of issues in its transport and storage. Practical temperatures and pressures should be attainable by sorption of methane into porous materials (*17*). Given that IRMOF-6 has an aperture (van der Waals dimension of 5.9 Å) (*18*) considered suitable for methane uptake, we sought to examine its viability in methane storage.

We first studied IRMOF-6 with the use of thermal gravimetric and gas sorption techniques to show that its framework has the high porosity and rigidity needed to allow maximum uptake of methane. The chloroform-exchanged IRMOF-6, $Zn_4O(R_6\text{-}BDC)_3\cdot(CHCl_3)_7$, was heated gradually to 800°C under inert atmosphere. A large and sharp weight loss of 50% of the original sample was observed below 100°C, which was attributed to liberation of all chloroform guests from the pores (calculated at 49%) (Fig. 3A). The evacuated framework has a stability range of 100° to 400°C, as evidenced by the fact that no additional weight loss was observed at those temperatures, after which the framework eventually decomposes.

The gas sorption isotherm measured for IRMOF-6 shows that it has a rigid framework, and can maintain its porosity in the absence of guests. An exact amount of the chloroform-exchanged IRMOF-6 was introduced into a microbalance apparatus and evacuated at room temperature and 10^{-5} torr, according to already published protocol (*19*). All of the chloroform guest molecules were removed from the pores. No additional weight change was observed upon overnight evacuation of the sample and heating to 150°C. At this point, the XRD of the evacuated form of IRMOF-6 was identical to that of the synthesized form, indicating the architectural stability of the evacuated framework. Studies of N_2 sorption at 78 K (Fig. 3B) revealed a reversible type I isotherm behavior characteristic of a microporous material. The plateau was reached at relatively low pressure with no additional uptake at relatively medium pressures (near condensation pressure $P/P_0 \sim 0.5$), confirming the homogeneity of the pores. By applying the Langmuir and Dubinin-Raduskhvich (DR) equations, the Langmuir surface area and pore volume, respectively, were estimated to be $S_{langmuir}$ = 2630 m^2/g and V_p = 0.60 cm^3/cm^3. The evacuated sample was also exposed to different organic vapors (CH_2Cl_2, C_6H_6, CCl_4, and C_6H_{12}) to give type I reversible isotherms (Fig. 3B) as well as pore volumes that converged to the same values (0.57 to 0.60 cm^3/cm^3) for all sorbates, further confirming the homogeneity of the pores.

The exceptionally high surface area and pore volumes observed for IRMOF-6, coupled with its appropriately designed aperture, made it an ideal candidate for methane stor-

age. Indeed, the methane sorption isotherm was measured in the pressure range 0 to 42 atm and room temperature and was found to have an uptake of 240 cm^3 at standard temperature and pressure (STP)/g [155 cm^3 (STP)/cm^3] at 298 K and 36 atm (Fig. 3C). This exceeds that of other crystalline materials including zeolite 5A (87 cm^3/cm^3) and other coordination frameworks [up to 213 cm^3 (STP)/g] (*17*, *20*, *21*). On the basis of volume for volume (v/v), the amount of methane sorbed by IRMOF-6 at 36 atm (which is regarded as a safe and cost-effective pressure limit) represents 70% of the amount stored in compressed methane cylinders in laboratories where much higher, unsafe levels of pressure (205 atm) are used. Reducing the pressure represents an advance that we believe will affect the future use of these materials in automobile fueling (*22*).

Methane uptake was also evaluated by testing IRMOF-1 and IRMOF-3 under the same conditions where their uptake was found to be lower [135 and 120 cm^3 (STP)/cm^3] than that of IRMOF-6—a significant difference that is attributable to the hydrophobic nature of C_2H_4 units in IRMOF-6. Thus, functionalizing the pores with larger hydrocarbons as illustrated in IRMOF-4, -5, and -7, may indeed result in even higher capacities. The most open members of this series (IRMOF-12 and -14) are also porous, in that they exhibit behavior similar to that described for IRMOF-6. In addition, they maintain their crystallinity in the absence of guests, as demonstrated by the coincidence of the XRD patterns of the synthesized material with those measured for the evacuated form of IRMOF-12 and -14.

The intrinsic value of this design approach lies in the ability to control and direct the reticulation of building blocks into extended networks in which specific properties can be targeted.

References and Notes

1. A. Stein *et al*., *Science* **259**, 1558 (1993).
2. P. J. Fagan, M. D. Ward, *Sci. Am*. **267**, 48 (1992).
3. O. M. Yaghi *et al*., *J. Solid State Chem*. **152**, 1 (2000).
4. M. Eddaoudi *et al*., *Acc. Chem. Res*. **34**, 319 (2001).
5. V. A. Russell *et al*., *Science* **276,** 575 (1997).
6. Y. H. Kiang *et al*., *J. Am. Chem. Soc.* **121**, 8204 (1999).
7. B. F. Hoskins, R. Robson, *J. Am. Chem. Soc.* **111**, 5962 (1989).
8. F. Serpaggi, G. Férey, *J. Mater. Chem*. **8**, 2749 (1998).
9. H. Li *et al*., *Nature* **402**, 276 (1999).
10. "Reticular" is an adjective, defined in Random House Webster Unabridged Dictionary as "having the form of a net; netlike." Isoreticular is defined as "having the same network topology."
11. All IRMOFs were formulated as $Zn_4O(Link)_3(DEF)_x$. [See (*23*) for details of elemental analyses.]
12. All the intensity data were collected on Bruker SMART CCD diffractometer with a graphite monochromated MoKα (λ = 0.71073 Å) radiation. Structures were solved by direct methods, and successive difference Fourier syntheses with SHELXTL software package. Final *R*1 values were calculated with $I > 2\sigma(I)$. Crystal data are as follows: IRMOF-2, cubic, space group *Fm*-3*m*, *a* = 25.772(1) Å, V = 17117(1) Å^3, Z = 8, *R*1 = 0.0976; IRMOF-3, cubic, *Fm*-3*m*, *a* = 25.747(1) Å, V = 17067(2) Å^3, Z = 8, *R*1 = 0.1160; IRMOF-4, cubic, *Fm*-3*m*, *a* = 25.849(1) Å, V = 17272(2) Å^3, Z = 8, *R*1 = 0.0706; IRMOF-5, cubic, *Pm*-3*m*, *a* = 12.882(1) Å, V = 2137.6(3) Å^3, Z = 1, *R*1 = 0.1181; IRMOF-6, cubic, *Fm*-3*m*, *a* = 25.842(2) Å, V = 17258(2) Å^3, Z = 8, *R*1 = 0.1325; IRMOF-7, cubic, *Pm*-3*m*, *a* = 12.914(3) Å, V = 2153.9(7) Å^3, Z = 1, *R*1 = 0.1957; IRMOF-8, cubic, *Fm*-3*m*, *a* = 30.092(2) Å, V = 27248(3) Å^3, Z = 8, *R*1 = 0.1691; IRMOF-9, orthorhombic, *Pnnm*, *a* = 17.147(1) Å, *b* = 23.322(1) Å, *c* = 25.255(1) Å, V = 10099.6(8) Å^3, Z = 4, *R*1 = 0.0802; IRMOF-10, [single crystals of sufficient quality to perform a single-crystal analysis study could not be obtained, but its observed x-ray powder diffraction pattern was the same as that observed for IRMOF-12 (below) and was confirmed by a simulated pattern for IRMOF-10 based on IRMOF-12 coordinates] cubic, *Fm*-3*m*, *a* = 34.281(2) Å, V = 40286(4) Å^3, Z = 8; IRMOF-11, trigonal, *R*-3*m*, *a* = 24.822(1) Å, *c* = 56.734(3) Å, V = 30272(3) Å^3, Z = 12, *R*1 = 0.0963; IRMOF-12, cubic, *Fm*-3*m*, *a* = 34.281(2) Å, V = 40286(4) Å^3, Z = 8, *R*1 = 0.1080; IRMOF-13, (same as treatment for IRMOF-10 but with the use of IRMOF-11) trigonal, *R*-3*m*, *a* = 24.822(1) Å, *c* = 56.734(3) Å, V = 30272(3) Å^3, Z = 12; IRMOF-14, cubic, *Fm*-3*m*, *a* = 34.381(13) Å, V = 40642(26) Å^3, Z = 8, *R*1 = 0.1914; IRMOF-15, cubic, *Im*-3*m*, *a* = 21.459(1) Å, V = 9882(1) Å^3, Z = 1, *R*1 = 0.1164; IRMOF-16, cubic, *Pm*-3*m*, *a* = 21.490(1) Å, V = 9925(1) Å^3, Z = 1, *R*1 = 0.1845. [See (*23*) for details.]
13. M. O'Keeffe, B. G. Hyde, *Crystal Structures I: Patterns and Symmetry* (Mineralogy Society of America, Washington, DC, 1996).
14. T. M. Reineke *et al*., *J. Am. Chem. Soc*. **122,** 4843 (2000).
15. M. J. Bennett, J. V. Smith, *Mater. Res. Bull*. **3,** 633 (1968).
16. N. Hüsing, U. Schubert, *Angew. Chem. Int. Ed.* **37**, 22 (1998).
17. V. C. Menon, S. Komarneni, *J. Porous Mater*. **5,** 43 (1998).
18. A van der Waals radius of C (1.70 Å) was used in determination of distance parameters [A. Bondi, *J. Phys. Chem*. **68**, 441 (1964)].
19. M. Eddaoudi *et al*., *J. Am. Chem. Soc*. **122,** 1391 (2000).
20. K. Seki, *Chem. Commun*. **16,** 1496 (2001).
21. S. Noro *et al*., *Angew. Chem. Int. Ed.*, **39,** 2081 (2000).
22. K. Seki *et al*., U.S. patent 5,862,796 (1999).
23. Single crystal XRD data and elemental microanalyses for IRMOF-2 through -16, including sorption and XRD data for IRMOF-12 and -14, are available as supplementary material on *Science* Online at www.sciencemag.org/cgi/content/full/295/5554/469/DC1.

24. Supported by NSF (M.O., O.M.Y.) and DOE (O.M.Y.). We thank D. Martin (University of Michigan, Material Sciences Engineering) for supplying a sample of the free R_6-BDC acid.

11 October 2001; accepted 6 December 2001

Spider Silk Fibers Spun from Soluble Recombinant Silk Produced in Mammalian Cells

Anthoula Lazaris,[1]* Steven Arcidiacono,[2] Yue Huang,[1] Jiang-Feng Zhou,[1] François Duguay,[1] Nathalie Chretien,[1] Elizabeth A. Welsh,[2] Jason W. Soares,[2] Costas N. Karatzas[1]

Spider silks are protein-based "biopolymer" filaments or threads secreted by specialized epithelial cells as concentrated soluble precursors of highly repetitive primary sequences. Spider dragline silk is a flexible, lightweight fiber of extraordinary strength and toughness comparable to that of synthetic high-performance fibers. We sought to "biomimic" the process of spider silk production by expressing in mammalian cells the dragline silk genes (*ADF-3*/*MaSpII* and *MaSpI*) of two spider species. We produced soluble recombinant (rc)–dragline silk proteins with molecular masses of 60 to 140 kilodaltons. We demonstrated the wet spinning of silk monofilaments spun from a concentrated aqueous solution of soluble rc–spider silk protein (ADF-3; 60 kilodaltons) under modest shear and coagulation conditions. The spun fibers were water insoluble with a fine diameter (10 to 40 micrometers) and exhibited toughness and modulus values comparable to those of native dragline silks but with lower tenacity. Dope solutions with rc–silk protein concentrations >20% and postspinning draw were necessary to achieve improved mechanical properties of the spun fibers. Fiber properties correlated with finer fiber diameter and increased birefringence.

The evolutionary survival of spiders has been tightly linked to the diversity, production, and use of silks (*1*–*3*). Orb-web spinning spiders have as many as seven highly specialized glands, each producing silk with different mechanical properties and functions (*4*–*6*). Dragline silk, used as the safety line and as the frame thread of the spider's web, is one of the strongest silks studied, being three times as tough as aramid fibers and five times stronger by weight than steel (*7*–*10*).

The protein core of dragline silk fibers is secreted as a mixture of two soluble proteins from specialized columnar epithelial cells of the major ampullate gland of orb-weaver

[1]Nexia Biotechnologies, Vaudreuil-Dorion, Quebec J7V 8P5, Canada. [2]Materials Science Team, U.S. Army Soldier Biological Chemical Command, Natick, MA 01760, USA.

*To whom correspondence should be addressed. E-mail: alazaris@nexiabiotech.com